

# 1. PETROGRAPHY AND MINERALOGY OF THE UPPERMOST MESSINIAN SECTION AND THE PLIOCENE/MIOCENE BOUNDARY AT SITE 975, WESTERN MEDITERRANEAN SEA<sup>1</sup>

Kathleen M. Marsaglia<sup>2</sup> and Jane S. Tribble<sup>3</sup>

## ABSTRACT

Ocean Drilling Program Site 975 is located near the base of the Menorca Rise in the South Balearic Basin of the western Mediterranean Sea. Coring at this site penetrated the Pliocene/Miocene boundary and recovered a sequence of sediments that represent the final stages of salt deposition and the transition from evaporitic to open marine conditions at the end of the Miocene (Messinian). Detailed petrographic observations and bulk mineralogical analyses by X-ray diffraction form the basis for preliminary interpretations of depositional environments for this section. Gypsum is thought to have been deposited in an evaporating basin below wave base. Cycles consisting of a clay layer overlain by gypsiferous chalk, laminated gypsum, and finally pinch-and-swell gypsum suggest upsection increases in salinity. The gypsum section is overlain by two exotic sand layers thought to mark events of fresher water (marine or meteoric) inflow to the basin. Gypsum deposition terminated and was replaced by inorganic precipitation of micritic calcite with periodic, variable dilution by fine-grained terrigenous sediment. The micritic sediments have fine, slightly wavy, laminations indicating either an algal/microbial mat origin, or varve-like fluctuations in deposition, perhaps in a deep basin. The Pliocene/Miocene boundary falls within an interval of banded micritic silty clays that reflect the final environmental fluctuations during the transition to the open marine conditions of the Pliocene.

## INTRODUCTION

Ocean Drilling Program (ODP) Site 975 is located off the Island of Menorca in the western Mediterranean (Fig. 1). At this site, a fairly complete Pliocene/Miocene boundary section was recovered (Comas, Zahn, Klaus, et al., 1996) that provides a unique opportunity to document facies changes across the transition from evaporitic to open marine conditions at the end of the Miocene (Messinian). Spot coring and poor recovery on previous Deep Sea Drilling Project (DSDP) legs precluded the successful recovery of intact upper Miocene and Pliocene/Miocene boundary sections at Sites 124, 133, 134, 371, and 372 in the western Mediterranean (Fig. 1). For example, biostratigraphy suggests that the Pliocene/Miocene contact occurred within a 20-m drilling gap at Site 124 off the south Balearic Plateau (Ryan, Hsü, et al., 1973), and that the Pliocene/Miocene boundary section was not recovered at Site 371 in the south Balearic Basin or at Site 372 on the Menorca Rise (Hsü, Montadert, et al., 1978). Even where the contact is thought to be undisturbed by drilling, such as at Site 134 to the east of Sites 124 and 371 across the Balearic Abyssal Plain, it is likely unconformable (Ryan, Hsü, et al., 1973). Although recovery was poor, a variety of upper Miocene lithologies were documented at these sites.

Herein we provide preliminary petrographic and mineralogical analyses of the latest Miocene evaporite and marine(?) sedimentary rocks recovered at Site 975. Our work builds on previous petrologic and geochemical studies conducted by Legs 13 and 47 shipboard and shore-based scientists, including the classic work of Ogniben (1955) in the Messinian sections of Sicily. The preliminary interpretations for Site 975 will be integrated with other biostratigraphic and geochemical studies (e.g., Iaccarino et al., Chap. 15; Iaccarino and Bossio, Chap. 42, both this volume), to provide a more detailed picture of this most interesting segment of Mediterranean history.

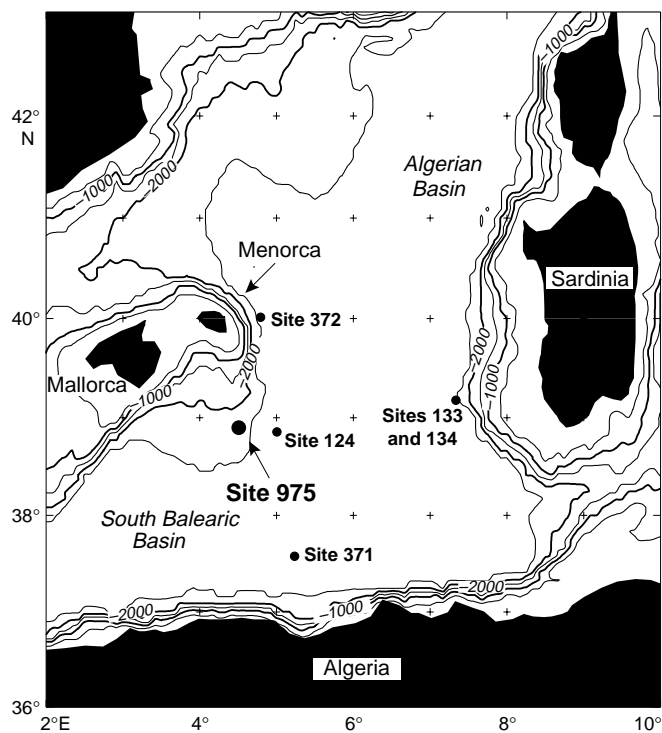


Figure 1. Location of DSDP and ODP sites in the Algerian and South Balearic Basins. See Nesteroff (1973, fig. 1, p. 674) and Garrison et al. (1978, fig. 1b, p. 572) for drilling/recovery/lithology summaries of DSDP Sites 124, 133, 134, 371, and 372.

## SITE 975 STRATIGRAPHY

Three stratigraphic units were defined at ODP Site 975 (see Shipboard Scientific Party, 1996b, fig. 4, p. 118). The youngest, Unit I, consists of ~305 m of Pleistocene to Pliocene nannofossil to calcareous clay and silty clay and nannofossil ooze with local organic-rich

<sup>1</sup>Zahn, R., Comas, M.C., and Klaus, A. (Eds.), 1999. *Proc. ODP, Sci. Results*, 161: College Station, TX (Ocean Drilling Program).

<sup>2</sup>Dept. of Geological and Environmental Sciences, Stanford University, Stanford, CA 94305, U.S.A. (Present address: Westport Technology Center International, 6700 Portwest Drive, Houston, TX 77024, U.S.A.) marsaglia@ibm.net

<sup>3</sup>University of Hawaii, School of Ocean and Earth Science and Technology, Honolulu, HI 96822, U.S.A. jtribble@soest.hawaii.edu

layers. Units II and III are Miocene in age. The contact between Units I and II (Miocene/Pliocene boundary) falls within a banded interval of calcareous silty clays and is marked by a compacted, intraclastic breccia or bioturbated zone overlain by sandy clay (Section 161-975B-33X-2, 131–134 cm; see in Shipboard Scientific Party, 1996b, p. 126, fig. 15). Unit II is composed of thinly interbedded to finely laminated micrite and micritic silty clay with minor calcareous silty sand. The Unit II/III boundary occurs just below a sandy interval at the top of the evaporite section (Fig. 2). Unit III is composed of finely laminated to pinch-and-swell gypsum and gypsiferous chalk with thin beds and laminae of clay, micrite-rich clay, foraminifer-rich and gypsum-bearing silty clay, and minor anhydrite.

**METHODS**

Samples were collected from cores recovered at Holes 975B and 975C. These were selected from evaporite, sandy, and calcareous facies from across the Pliocene/Miocene boundary, but emphasizing Units II and III. Billets of more lithified units were first photographed and micro-sampled for geochemical and mineralogical analyses before impregnation with blue-dyed epoxy and ground to 30 μm in thickness. Thin sections prepared from the billets were then examined with a petrographic microscope. The carbonate and evaporite classification schemes and terminology used in this study are outlined in Carozzi (1993).

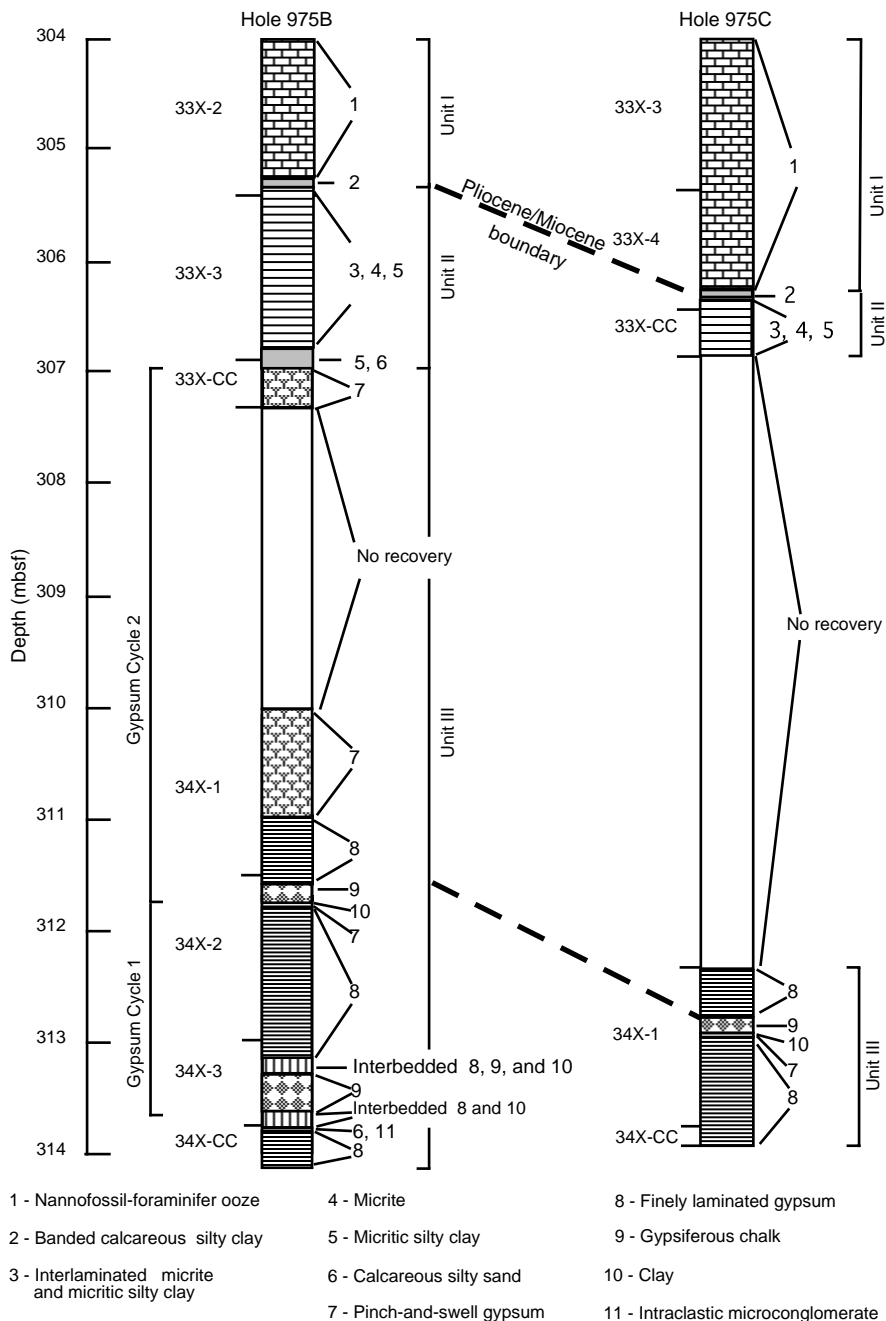


Figure 2. Stratigraphic representation of Units I, II, and III in Holes 975B and 975C. Unrecovered sections are by convention shown at the base of Cores 161-975B-33X and 975C-33X, but a missing section could actually exist anywhere within the cored interval. Gypsum cycles 1 and 2 are indicated, as well as probable correlation lines (dashed) between the cores.

X-ray diffraction (XRD) was used to determine bulk mineralogy. Roughly one third of the samples for this study were analyzed on shipboard according to methods described in the Leg 161 *Proceedings of the Ocean Drilling Program, Initial Reports*, “Explanatory Notes” chapter (Shipboard Scientific Party, 1996a). The remaining samples were analyzed at the University of Hawaii (UH) using a Scintag PAD V powder diffractometer. The samples were continuously scanned from  $2^\circ 2\theta$  to either  $40^\circ$  or  $60^\circ 2\theta$ , using a chopper increment of  $0.03^\circ$  and a scan speed of  $1^\circ 2/\text{min}$ . Unfiltered  $\text{CuK}\alpha$  radiation was used with a tube voltage of 45 kV and a tube current of 40 mA.

The relative abundances of total clay minerals, quartz, plagioclase, and calcite, normalized to 100%, were estimated for the bulk samples using a routine developed at UH. The routine uses a simultaneous linear equation algorithm that accounts for peak overlap (Karlak and Burnett, 1966) and was calibrated using a series of multicomponent mixtures as external standards. Details of the quantification method are given in Wilkens et al. (1992). In addition to the four phases quantified (clay minerals, quartz, feldspar, and calcite), the relative intensities of the main X-ray peaks for other identified phases were determined. These relative intensities are simply measures of peak height relative to the tallest peak in the pattern and should not be compared numerically with the weight percentages.

## PETROGRAPHIC DESCRIPTIONS

### Units I and II

One thin section of a sandy interval near the base of Unit I and three thin sections from two sandy beds at the base of Unit II were examined. Petrographic descriptions of these samples are given in Table 1 and photomicrographs are shown in Plate 1. The Unit II sandy beds are separated by a 4- to 5-cm bed of gypsum-bearing micritic silty clay within a 17-cm interval of core directly above the Unit II/Unit III contact (Figs. 2, 3A, B). When Core 161-975B-33X was cut into sections, it was split within this micritic bed so that it occurs at the base of Section 975B-33X-3 and at the top of Section 975B-33X-CC (Fig. 3A, B).

Thin sections were prepared from the base (Section 161-975B-33X-CC, 9–10 cm) and the top (Section 975B-33X-CC, 3–5 cm) of the lower sandy interval (Fig. 3B). Both samples show similar compositional ranges with an upsection decrease in sorting. XRD results (Table 2) indicate variable amounts of celestite ( $\text{SrSO}_4$ ) and gypsum in this sandy interval.

### Unit III

A series of thin sections were prepared from Unit III cores from Holes 975B and 975C. These provide the basis for characterizing the spectrum of evaporite lithofacies identified by shipboard studies (see Fig. 2: e.g., pinch-and-swell gypsum [7; referred to as nodular gypsum in the shipboard studies], finely laminated gypsum [8], and gypsiferous chalk [9]). We have further subdivided the finely laminated gypsum into planar laminated (8a), planar-wavy laminated (8b), planar-cumulus (8c), and crenulated (8d) varieties. Unfortunately some lithofacies are not represented in our sample suite. Thin sections were not made of clay (10) interbeds because these intervals were depleted for paleontological studies. One very thin interval of what appeared to be intraclastic gypsum (11), which was composed of thin flakes similar to the laminated gypsum, was depleted in an attempt to make a thin section for shipboard study.

Some of these lithofacies (10 through 7) are organized in two broad cycles (Fig. 2) starting at the base with clay or micrite-rich clay (10), followed by laminated to thinly bedded gypsiferous chalk (9), finely laminated gypsum (8), and topped by pinch-and-swell gypsum (7). Figures 4A and B illustrate these components in a correlative

interval recovered at Holes 975B and 975C. Planar laminae are most common at the base of the laminated interval within each cycle, and planar-wavy laminae become more common toward the top of the interval, where they evolve into planar-cumulus laminae and finally pinch-and-swell structures. These are described below in detail.

### *Gypsiferous Chalk*

The gypsiferous chalk (9; Figs. 4A and B) consists predominantly of large euhedral to anhedral gypsum crystals in a micritic matrix. The matrix material consists of micritic carbonate, nannofossils, and clay minerals(?) with a few percent foraminifers (Pl. 2, fig. 1) and foraminifer fragments, and traces of altered volcanic glass. The large gypsum crystals range up to 5 mm in length and often have fine inclusions of matrix material, including foraminifers and nannofossils. They exhibit no distinct zoning and may be intergrown. The long axes of gypsum crystals are often subhorizontal to horizontal (Pl. 2, fig. 2), but can show a range of orientation in some intervals (Pl. 2, fig. 1). Where crystals are in contact, they have undergone pressure solution and exhibit stylolitic contacts (Pl. 2, fig. 2). Locally, euhedral crystals exhibit irregular, matrix-rich overgrowths that extend out into the surrounding matrix. In the core photographs (Fig. 4A, B) subtle internal lamination and bedding features can be seen within the gypsiferous chalk intervals. These layers are defined by changes in the relative abundances of gypsum and matrix, by changes in gypsum crystal size, or by the presence of stellate clusters and subvertical bands of intergrown gypsum crystals.

### *Finely Laminated Gypsum*

The textures of laminated gypsum (8) vary as a function of the morphology of the upper surface of the laminae from planar (Fig. 5A), to planar-wavy (Fig. 5A), to planar-cumulus (Fig. 5B, C). We introduce the term cumulus because these structures resemble cumulus clouds. Alternative descriptive terms do not accurately describe these features: for example, “grass-like” and “cauliflower” have been applied to more pointed, vertical arrangements of selenitic crystals, and “cavoli,” is applied to more rounded fan-like arrangements of crystals (e.g., Richter-Bernburg, 1973). Garrison et al. (1978) described similar laminae at Site 372 as simply “irregular shaped gypsum crusts.”

In the instance of planar lamination, where both the upper and lower contacts of the laminae are planar, the gypsum usually consists of silt-sized elongate crystals aligned horizontally. Visible millimeter-scale lamination in the core reflects subtle variations in intercrystalline porosity, grain size and percent of nongypsum components in thin section. The nongypsum components include silt-sized quartz, biotite flakes, and whole and fragmented foraminifers. The clastic nature of these laminae is particularly evident in micrite- and clay-rich laminae, where gypsum grains are outlined. Gypsum grains include euhedral and broken prismatic to lenticular crystals showing various degrees of rounding. Because of the horizontal alignment of crystals where the gypsum is relatively pure, it takes on a felted appearance. Very thin, matrix-rich laminae resemble stylolites and may be zones of enhanced pressure solution (Pl. 2, fig. 3). In thicker, more homogeneous laminae, faint lamination is defined by wispy stringers and pods of matrix material. These matrix “blebs” are disseminated, but show horizontal alignment.

Where planar-wavy laminae are present, they alternate with intervals of planar laminae (e.g., Fig. 5A). A typical planar-wavy lamina begins with a few millimeters of relatively pure, silt to fine sand size (0.05–0.125 mm) rectangular gypsum crystals that are aligned parallel to bedding. Up-section in the top few millimeters of the lamina, they become coarser, more randomly oriented, and equigranular, but where rectangular or prismatic, take on a more subvertical orientation. In some cases the change to coarser crystals is marked by a planar-

**Table 1. Petrographic descriptions of sandy intervals.**

Core, section, interval (cm)	Name	Texture	Grain size	Major components	Minor components	Matrix composition	Cement
161-975B-33X-2, 3-4	Foraminifer-nannofossil ooze.	Grain- to matrix-supported.	Sand to clay.	Whole and fragmented planktonic foraminifers.	Quartz with Fe-coatings; zircon; glauconite; feldspar; phosphatic debris; quartz-mica tectonite lithic fragments.	Nannofossils; clay minerals; Fe-oxides; opaque minerals.	Carbonate and glauconite in foraminifers.
33X-3, 143-144	Carbonate-volcaniclastic lithic sandstone.	Grain- to matrix-supported; matrix-rich; well rounded to subangular grains.	Granule to clay.	Roughly equal proportions of volcanic and carbonate lithic fragments (black, tachylitic and altered microlitic and lathwork volcanic debris; micrite, oncolitic micrite, microsparite, biomicrosparite, pelletal micrite and microsparite, calcarenite); carbonate lithic fragments contain planktonic foraminifers and tintinnids(?).	Quartz; plagioclase; opaque minerals.	Silt-sized whole and fragmented foraminifers; altered glass; micrite; nannofossils (?); clay minerals.	
33X-CC, 9-10	Biocalcarene with terrigenous sand.	Grain-supported; laminated; moderately well sorted.	Sand.	Planktonic foraminifers; monocrystalline and polycrystalline quartz; lithic fragments of micrite, shale/slate, quartz-mica tectonite, polycrystalline mica.	Red algae; glauconite; phosphatic bone fragments(?); pellets; biotite; plagioclase; coarse carbonate; garnet; celestite(?).	Rare.	Microcrystalline celestite(?).
33X-CC, 3-5	Biomicrite with terrigenous sand.	Matrix-to grain-supported; laminated (alternating laminae are more bioclast- and quartz-rich).	Sand to clay.	Whole and fragmented planktonic foraminifers; monocrystalline and polycrystalline quartz; lithic fragments of shale/slate, siltstone, sedimentary chert, quartz-mica tectonite, polycrystalline mica, micrite, altered volcanic glass.	Echinoderm; phosphatic debris; biotite; plagioclase; coarse carbonate; garnet, fragments of shale/slate.	Micrite; clay minerals.	Common celestite protonodules(?).

**Table 2. Site 975 X-ray mineralogy, Units I and II.**

Core, section, interval (cm)	Type	Depth (mbsf)	Clay minerals (wt%)	Quartz (wt%)	Feldspar (wt%)	Calcite (wt%)	Dolomite (rel. int.)	Celestite (rel. int.)	Gypsum (rel. int.)
161-975B-									
Unit I									
33X-2, 3	1	303.93	31	8	0	62	1	0	0
33X-2, 12	1	304.02	32	6	0	62	1	0	0
33X-2, 68	1	304.58	43	9	1	47	4	0	0
33X-2, 78	1	304.68	37	9	0	54	3	0	1
33X-2, 102	2a	304.92	65	15	1	18	22	0	0
33X-2, 126	2b	305.16	49	10	1	40	5	0	2
33X-2, 130	2a	305.20	72	13	1	14	11	0	0
Unit II									
33X-2, 132	2b	305.22	58	6	1	35	7	0	0
33X-2, 135	2a	305.25	62	14	2	23	5	0	0
33X-2, 139	2b	305.29	48	9	1	42	0	0	0
33X-3, 3	3	305.43	33	29	0	38	49	17	0
33X-3, 9	3	305.49	47	9	1	43	7	0	0
33X-3, 14	3	305.54	39	10	1	50	3	0	0
33X-3, 63	4	306.02	0	0	0	100	3	0	0
33X-3, 68	4	306.07	0	5	0	95	11	0	0
33X-3, 86	5	306.25	64	18	1	17	27	0	0
33X-3, 92	5	306.31	52	16	1	30	19	0	0
33X-3, 105	5	306.44	59	5	1	36	4	0	0
33X-3, 117	3	306.56	47	8	1	44	13	0	0
33X-3, 143	6	306.82	46	15	5	34	17	0	0
33X-3, 143	6	306.82	38	13	3	46	17	0	0
33X-CC, 1	5	306.86	39	4	1	56	5	0	7
33X-CC, 3	6	306.88	37	17	0	46	11	23	tr
33X-CC, 7	6	306.92	36	34	0	30	25	100	0
33X-CC, 9	6	306.94	31	18	3	48	9	4	100

Notes: Sediment types: 1 = nannofossil-foraminifer ooze; 2 = banded calcareous silty clay, a = dark interval, b = light interval; 3 = interlaminated micrite and micritic silty clay; 4 = micrite; 5 = micritic silty clay; 6 = calcareous silty sand. Rel. int. = intensity of peak relative to largest peak present in pattern.

discontinuous, matrix-rich seam that may be slightly stylolitized. Intracrystalline and intercrystalline porosity is present throughout the lamina. The coarse, interlocking gypsum is abruptly overlain by a darker (in thin section) matrix-rich zone (Pl. 3, fig. 1). This overlying “matrix” material is a mixture of clay minerals(?), silt-sized carbonate including nannofossils, and rectangular to anhedral gypsum crystals. As in the planar laminations, the gypsum grains include euhedral and broken, prismatic to lenticular crystals showing various degrees of rounding. The matrix also contains traces of quartz silt, biotite flakes, and whole and fragmented foraminifers. This matrix material has a definite detrital appearance, with horizontal alignment of the long axes of gypsum grains, and its contact with the underlying coarse gypsum appears to be erosional. This matrix-rich zone passes upward gradationally into relatively pure gypsum.

In the case of planar-cumulus laminae (Fig. 5B, C) the coarsely crystalline cap observed in the planar-wavy laminae is better developed and thicker (up to 1–2 cm). Again, crystal size and degree of vertical orientation increase up through the structure. The equigranular to rectangular crystals are interlocking and can range up to 0.5 mm in length (Pl. 3, fig. 2). The crystals are locally replaced by irregular patches of fibroradiating quartz. The coarsely crystalline, massive gypsum within individual “clouds” is abruptly overlain by a laminated matrix. The matrix onlaps and drapes the coarsely crystalline, irregular “cumulus” topography at depositional to erosional contacts (Pl. 3, fig. 2). The matrix is essentially the same composition as that described above and includes detrital gypsum. In many instances the planar-cumulus laminae are actually compound features directly built upon thin, planar-wavy laminae. They grade upward into pinch-and-swell structures, and locally form keel-like structures (miniature depression cones) where they apparently sank into the surrounding sediment.

One thin interval of crenulated gypsum (8d), where laminae boundaries are irregular in a parallel fashion, is present near the base of Core 161-975B-34X (Fig. 6). These laminae differ from those described above in the following ways: (1) the matrix is composed of granular carbonate (slightly irregular and circular in shape) with high relief (probably dolomite, see Table 3), (2) gypsum crystals (both detrital and possible in situ precipitates) are predominantly lenticular

in shape (Pl. 2, fig. 4), and (3) the development of stylolitization is more extreme.

#### *Pinch-and-Swell Gypsum*

Pinch-and-swell gypsum (7) consists of thin beds or laminae of massive gypsum separated by finely laminated matrix. The massive gypsum layers exhibit pinch-and-swell structure with matrix concentrated in the “pinch” zones (Fig. 7). These pinch-and-swell structures are often offset and nested, resulting in vertically alternating “pinch” zones and “swell” zones. The matrix appears to drape and onlap massive gypsum “swells.”

The massive gypsum consists of interlocking coarse crystals of gypsum with high (15%–20%) intercrystalline and intracrystalline porosity (Pl. 3, fig. 3). The gypsum crystals are equant to rectangular in shape and where elongate, have a subvertical orientation. The nature of intercrystalline contacts is hard to evaluate because they may have been modified by pressure solution.

The silty matrix is laminated to massive and exhibits clastic textures modified by compaction and pressure solution. Silt-sized, rectangular gypsum crystals are the dominant component with rare, small foraminifers (whole and fragmental), biotite flakes, and quartz grains. Carbonate is rare to common, and occurs as fine micrite (associated with clay minerals?), isolated rhombs, and “ring”-shaped crystals, which are interpreted to be recrystallized nannofossils. Flattened pods of micrite are present locally. In thin section, matrix can be seen to interfinger with massive gypsum on the margins of some “swell” structures (Pl. 3, fig. 4). Thinning of matrix intervals across “swells” appears to be a depositional artifact that may have been enhanced by subsequent pressure solution and differential compaction. The surfaces of “swells” appear eroded and larger clasts of gypsum are scattered in the matrix along this contact.

## MINERALOGICAL ANALYSES

### Units I and II

A generalized lithologic column for the base of the Pliocene (Unit I) and the uppermost Miocene (Unit II; Fig. 8) shows the major

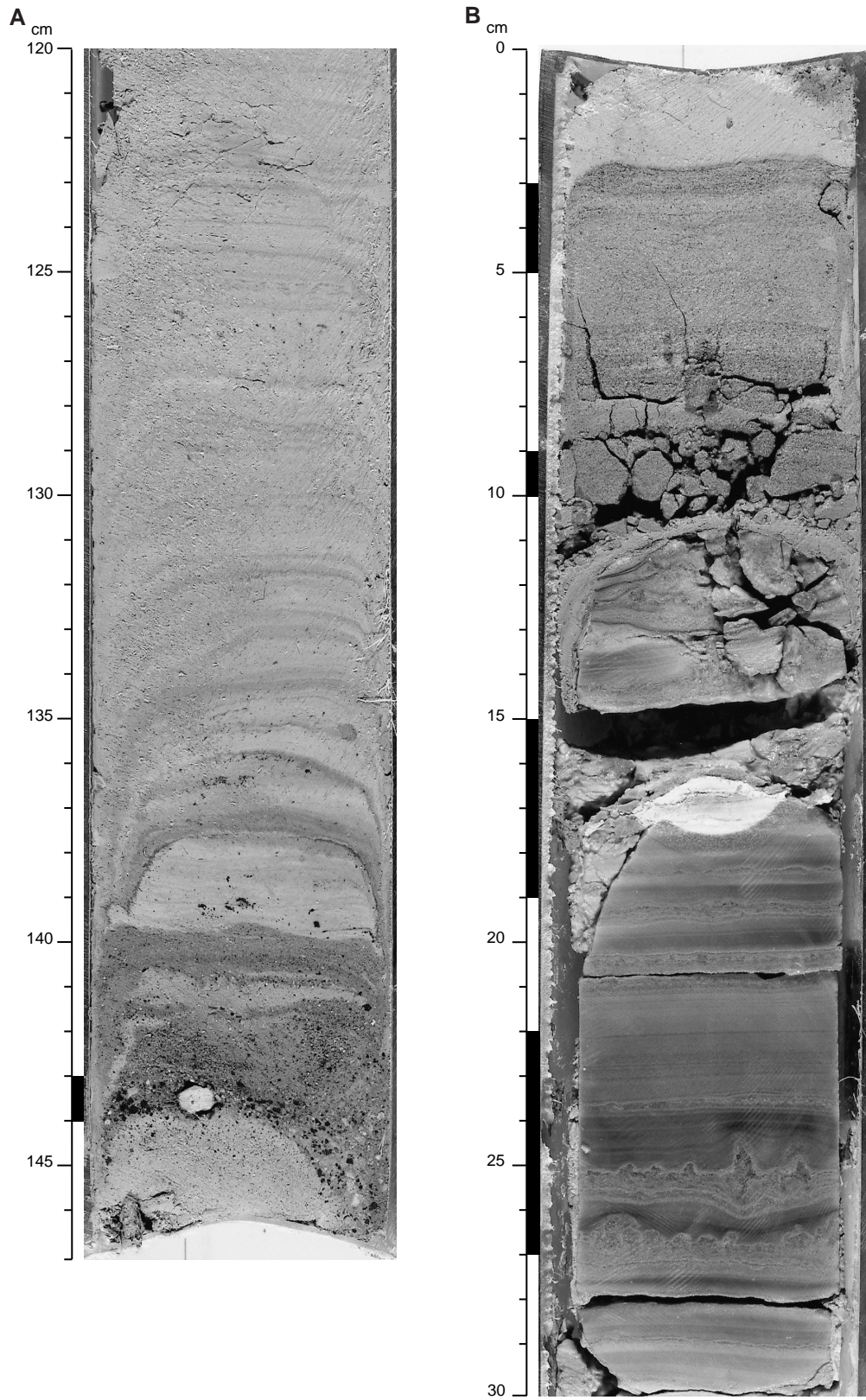


Figure 3. Core photographs of (A) Section 161-975B-33X-3, 120–147 cm, and (B) Section 975B-33X-CC, 0–30 cm. Thin-section sample intervals are marked with black shading to the right of the scale.

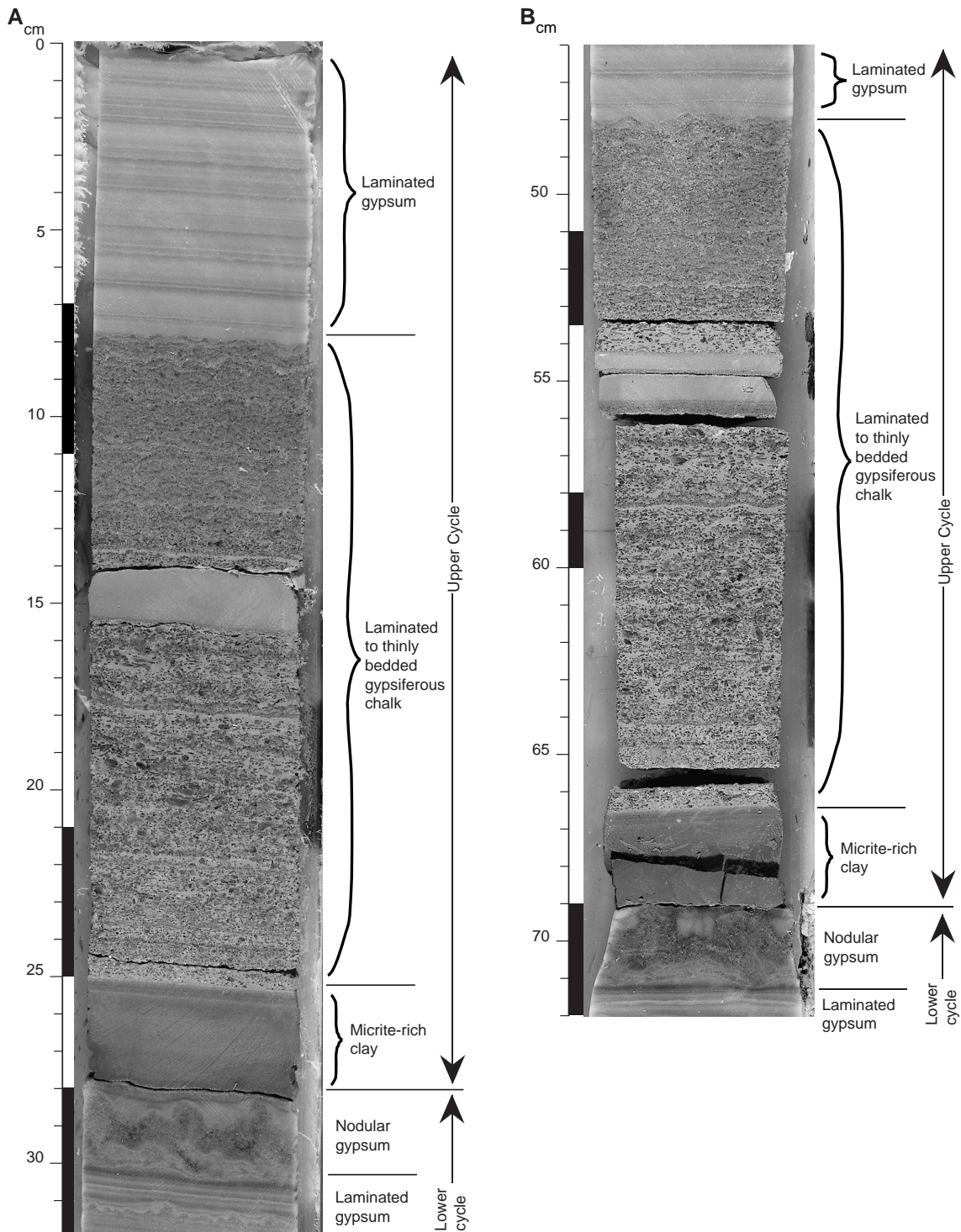


Figure 4. Photographs of gypsum cycles in Holes 975B and 975C. Thin-section sample intervals are marked with black shading to right of scale. **A.** Section 161-975B-34X-2, 0–32 cm. Contact between gypsum cycles 1 and 2 (as defined in Figure 2) is at 28 cm. Components of gypsum cycle 2: thin clay bed (25–28 cm), laminated to thinly bedded gypsiferous chalk (8–25 cm), and planar-laminated gypsum (0–8 cm; note few planar-wavy laminae at 3 and 5.5 cm). Components of gypsum cycle 1: nodular gypsum (28–30 cm) and planar-laminated gypsum (30–32 cm; note planar-cumulus lamina at 31 cm). **B.** Section 161-975C-34X-1, 46–72 cm. Contact between gypsum cycles 1 and 2 (as defined in Figure 2) is at 69 cm. Components of gypsum cycle 2: thin clay bed (66.5–69 cm), laminated to thinly bedded gypsiferous chalk (48–66.5 cm), and planar-laminated gypsum (46–48 cm). Components of gypsum cycle 1: nodular gypsum (69–71 cm), and planar-laminated gypsum (71–72 cm).

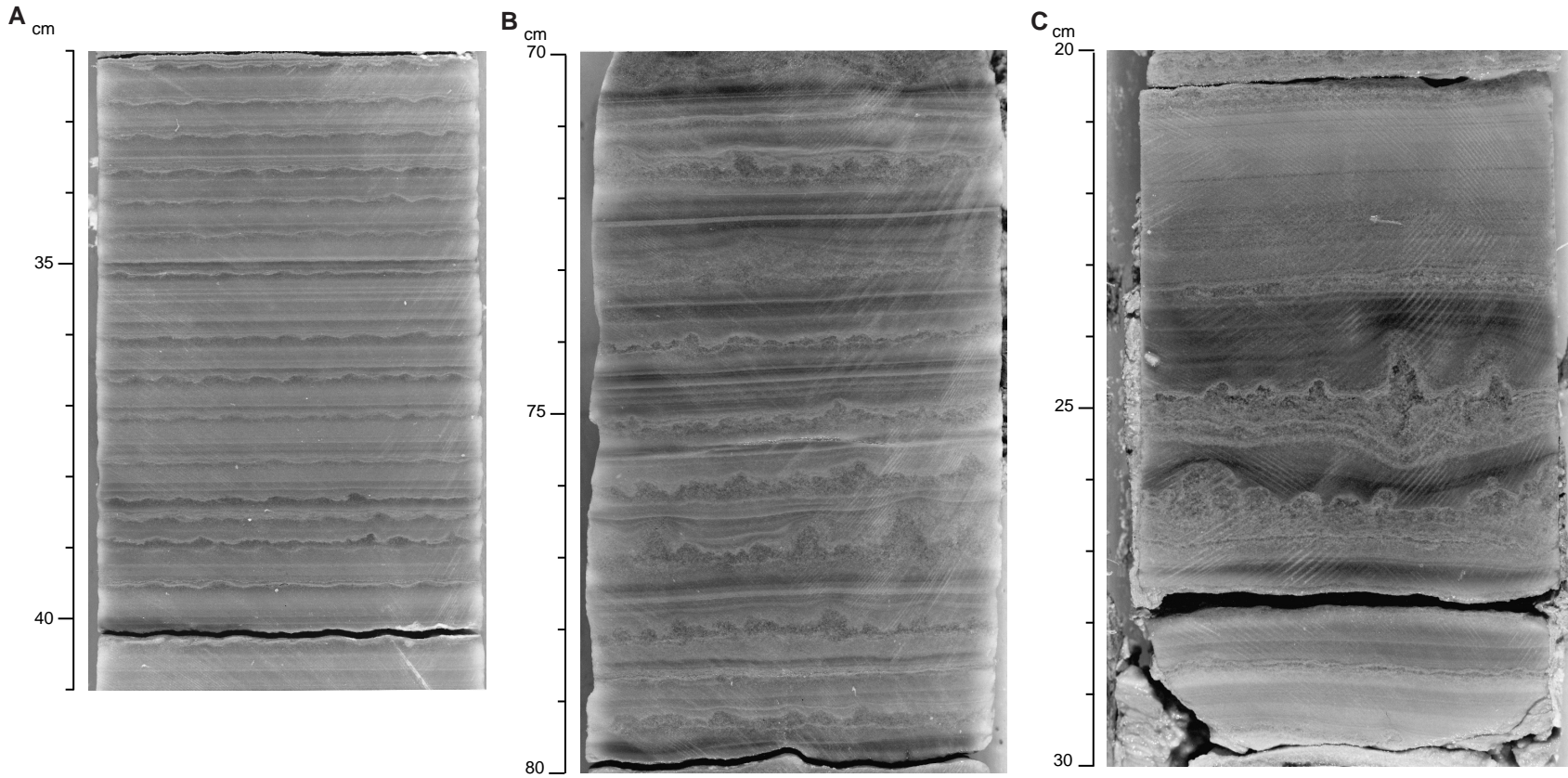


Figure 5. Photographs detailing the fine millimeter to submillimeter structure of laminated gypsum. **A.** Planar to wavy-planar laminae in gypsum cycle 2, Section 161-975C-34X-1, 32–41 cm. **B.** Planar-cumulus laminae in gypsum cycle 1, Section 161-975C-34X-1, 70–80 cm. Top of photograph (70–70.5 cm) is a thin bed of pinch-and-swell gypsum pictured in Figure 4B. **C.** Planar-cumulus laminae, Section 161-975B-33X-CC, 20–30 cm (see also Fig. 3B).

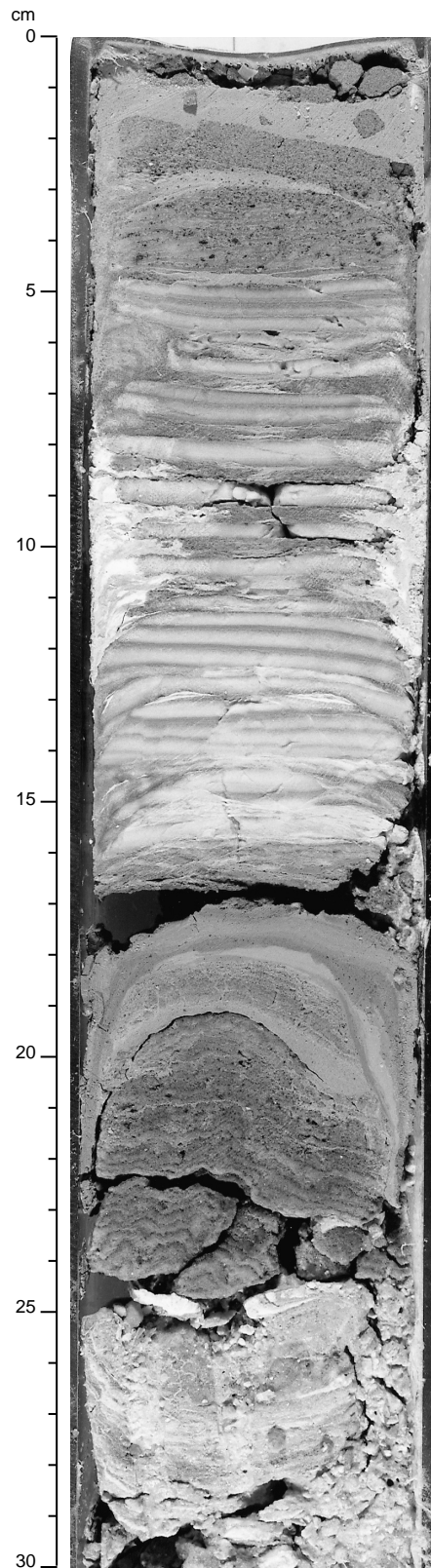


Figure 6. Crenulated gypsum at 19–24 cm and possible thin bed of intraclastic (rip-up clasts?) microconglomerate at 2–4 cm, separated by planar-laminated gypsum. Section 161-975B-34X-CC, 0–30 cm.

changes in sediment type during the transition from the Messinian evaporative environment, during which the gypsum-bearing sediments of Unit III dominated, to the pelagic, open-water environment of the Pliocene. Semi-quantitative XRD results (Table 2) document the significant mineralogical changes associated with these lithologic variations. In Table 2, sample types are keyed to the lithologies given in Figures 2 and 8. Figure 9 shows depth profiles of the major phases present. Departures from the relatively uniform mineralogy characteristic of the lower Pliocene (see Tribble and Wilkens, Chap. 8, this volume) are apparent at a depth of 304.92 mbsf, above the Pliocene/Miocene boundary defined on the basis of planktonic foraminifers (305.22 mbsf; Iaccarino et al., Chap. 15, this volume). The abundance of clay minerals and, to a lesser extent, quartz, increase at the expense of calcite, and there is also an increase in the relative intensity of the dolomite peak. This excursion in bulk mineralogy corresponds to a sample from a parallel-laminated interval in Section 161-975B-33X-2 at about 102 cm (see Core 975B-33X photograph in Comas, Zahn, Klaus, et al., 1996, p. 525).

Below this depth, bulk mineralogy varies dramatically between compositions characteristic of the calcite-rich micritic intervals, and those of the clay- and quartz-rich silty clays and the sands. Intermediate lithologies, although quite different in terms of sediment components, have bulk mineralogies that are not too dissimilar to those of the overlying pelagic sediment. These variations in mineralogy are most distinct in plots of mineral ratios (Fig. 10). The interval surrounding the Pliocene/Miocene boundary is characterized by alternations of dark and light sediment (Fig. 8; also see Shipboard Scientific Party, 1996b, fig. 15, p. 126). Dark bands are marked by relatively high ratios of clay/calcite and quartz/calcite, low calcite abundance, and slightly elevated dolomite intensities (Figs. 9C, D and 10A, B). Light bands have clay/calcite ratios slightly above, and quartz/calcite ratios similar to, the background levels defined by the overlying pelagic sediments (Fig. 10A, B). Calcite concentrations are distinctly higher in the light bands than in the dark bands, but still somewhat lower than in the overlying pelagic sequence. Dolomite intensities are at background levels (Fig. 9C, D).

Below the banded interval, the core contains about 60 cm of finely interlaminated micrite and micritic silty clay (Fig. 8; see also Shipboard Scientific Party, 1996b, fig. 18, p. 127). Sample 161-975B-33X-3, 3 cm, in this interval has unusually high concentrations of quartz and dolomite, as well as a significant percentage of celestite (Table 2; Fig. 9B, D). The abundance of dolomite and celestite may indicate the presence of a diagenetic front. Brines diffusing upward from the evaporative facies would provide  $\text{SO}_4^{2-}$  for reaction with  $\text{Sr}^{2+}$  possibly released by recrystallization of carbonates and result in precipitation of celestite. Dolomite is also a common diagenetic product of reaction of brines with carbonate minerals, although its coexistence with a high-quartz concentration indicates the possibility of a detrital source for the dolomite, as has been suggested for other Leg 161 sites (Tribble and Wilkens, Chap. 8, this volume) and for stoichiometric dolomite from Site 372 (Pierre and Fontes, 1978). The other two samples from the interval of interlaminated micrite and micritic silty clay have bulk mineralogies similar to the background Pliocene sediments (Figs. 9 and 10).

Below the interlaminated interval there are about 50 cm of interbedded micrite and micritic silty clay (Fig. 8; see also Shipboard Scientific Party, 1996b, fig. 17, p. 127). Samples from this interval represent the end-member compositions for the finely interlaminated sequences above and below. Two samples of micrite were analyzed (Samples 161-975B-33X-3, 63 cm and 68 cm; see Table 2). Both are nearly pure calcite, with only minor admixtures of dolomite, and in one case, quartz. No clay minerals were detected in the micrite (Fig. 9). The micritic silty clay end-member is represented by Samples 975B-33X-3, 86 and 92 cm (Table 2). These samples are enriched in total clay minerals, quartz, and dolomite and have low calcite abundance (Fig. 9). A third sample of micritic silty clay (Sample 975B-

**Table 3. Site 975 X-ray mineralogy, Unit III.**

Core, section, interval (cm)	Type	Depth (mbsf)	Clay								
			minerals (wt%)	Quartz (wt%)	Feldspar (wt%)	Calcite (wt%)	Dolomite (rel. int.)	Gypsum (rel. int.)	Calcite (rel. int.)	Quartz (rel. int.)	Anhydrite (rel. int.)
161-975B-											
33X-CC, 15	8b	307.00					0	100	5	00	
33X-CC, 15	8b	307.00					0	100	3	0	0
33X-CC, 15	8b	307.00					0	100	0	0	0
33X-CC, 19	8b	307.04					0	100	0	0	0
33X-CC, 21	8b	307.06					0	100	4	tr	0
33X-CC, 22	8a	307.07					0	100	3	0	0
33X-CC, 22	8b	307.07					0	100	0	0	0
33X-CC, 31	8b	307.16					0	0	0	0	100
33X-1, 9	7	310.09					0	100	0	0	0
34X-1, 26	7	310.26					0	100	5	0	0
34X-1, 120	8a	311.20					0	100	0	0	0
34X-2, 7	9	311.57					0	100	4	1	0
34X-2, 7	8a	311.57					0	100	0	0	0
34X-2, 21	9	311.71					4	100	11	2	0
34X-2, 26	10	311.76	80	10	1	10	14	14	80	100	0
34X-2, 28	8a	311.78					0	100	0	0	0
34X-2, 28	8c	311.78					0	100	0	tr	0
34X-2, 28	8a	311.78					0	100	tr	0	0
34X-2, 28	7	311.78					0	100	0	0	0
34X-3, 17	8a	313.15					0	100	0	0	0
34X-3, 27	9	313.25					17	100	72	15	0
34X-3, 28	5,9	313.26					3	100	14	4	0
34X-3, 55	9	313.53					0	100	4	0	0
34X-CC, 1	11	313.75					7	100	31	3	0
34X-CC, 4	11	313.78					4	100	4	tr	0
34X-CC, 14	8a	313.88					0	100	0	0	0
34X-CC, 19	8d	313.93					7	100	0	1	0
34X-CC, 19	5	313.93	20	15	0	66	6	69	100	22	0
161-975C-											
34X-1, 9	8a	311.15					0	100	3	1	0
34X-1, 37	8a,b	311.42					0	100	0	0	0
34X-1, 37	8a,b	311.42					0	100	0	0	0
34X-1, 51	7	311.6					tr	100	4	1	0
34X-1, 67	8c	311.76					0	100	0	0	0
34X-1, 70	8c	311.78					0	100	0	0	0
34X-1, 70	8c	311.78					0	100	0	0	0
34X-1, 142	8b	312.51					0	100	6	1	0
34X-1, 142	8b	312.51					0	100	0	0	0

Notes: Sediment type: 5 = micritic silty clay; 7 = pinch-and-swell gypsum; 8 = finely laminated gypsum, a = planar, b = wavy-planar, c = planar-cumulus, d = crenulated; 9 = gypsiferous chalk; 10 = clay; 11 = intraclastic microconglomerate. Rel. int. = intensity of peak relative to largest peak present in pattern.

33X-3, 105 cm) has a somewhat intermediary composition (Table 2; Fig. 9). This interbedded interval is underlain by another finely inter-laminated interval (Fig. 8).

The remaining section of Unit II consists primarily of sand-rich layers described in the petrologic description section above. The carbonate-volcaniclastic sand at a depth of 141–143 cm in Section 161-975B-33X-3 is noteworthy for its unusually high feldspar content (Table 2). Sample 975B-33X-CC, 7 cm, from the calcareous/terrigenous sand, contains abundant quartz, dolomite, and celestite (Table 2). The only X-ray detectable gypsum in Unit II sediments is from samples from Section 975B-33X-CC (Table 2).

The detrital component of Unit II sediments varies considerably in quantity, but a depth plot of the quartz/clay ratio (Fig. 10C) indicates a general constancy in the composition of the detrital material from the latest Miocene through the earliest Pliocene. The quartz-rich samples of the calcareous/terrigenous sand from Section 161-975B-33X-CC and the single sample from Section 975B-33X-3, 143 cm, are the only exceptions. In addition, although individual clay minerals were not quantified, illite and chlorite were consistently present in all clay-bearing samples.

A major difference between the sediments of Unit II and the overlying Pliocene Unit I is one not detectable via XRD: the source of the calcite. Figure 11 shows the cumulative percentages of all calcite components detected in smear slides for these sediments. At the same depth as the shallowest shift in mineralogy (304.92 mbsf), the percentage of foraminifers drops to near-zero values, the abundance of nanofossils drops markedly, and micrite becomes an important sedimentary constituent. Foraminifers ( $\pm$  bioclasts) are again abundant in the sand-rich lithologies near the base of Unit II.

### Unit III

Mineralogy for Unit III samples is reported in Table 3. For the gypsiferous sediments of Unit III, the quantification routine could not be used. For these samples, relative peak intensities are listed for the major phases. Weight percentages are reported only for two samples of clay and micritic silty clay that were interbedded with the gypsum. One sample of pure anhydrite was found (Sample 161-975B-33X-CC, 31 cm) corresponding to an interval of relatively soft, laminated sediment between two intervals of finely laminated gypsum. The remaining samples are all dominated by gypsum. Samples of gypsiferous chalk have the highest concentrations of nongypsum components, which include calcite, dolomite, and quartz. Pinch-and-swell and finely laminated varieties of gypsum generally have little or no detectable nongypsum components. The two samples of intraclastic microconglomerate (Samples 975B-34X-CC, 1 cm and 4 cm) also have relatively high concentrations of calcite, dolomite, and quartz.

## DISCUSSION

### Site 975 Evaporite Facies

Most of the laminated evaporite intervals at Site 975 consist of what appears to be detrital gypsum, in that the fragments are angular to slightly rounded but generally are rectangular in shape and appear to be broken. Possible sources of gypsum crystals include precipitates that nucleate at the water surface and settle through the water column or nucleate as crusts on the bottom at the sediment-water interface (Schreiber, 1978, 1988). Both may be reworked and trans-

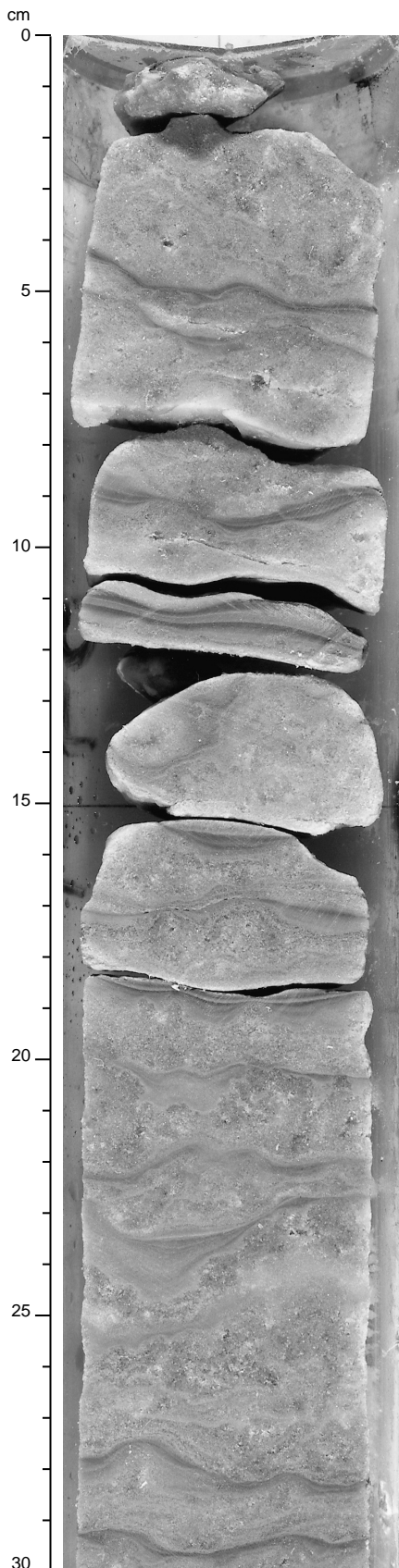


Figure 7. Pinch-and-swell gypsum. Section 161-975B-34X-1, 0–30 cm.

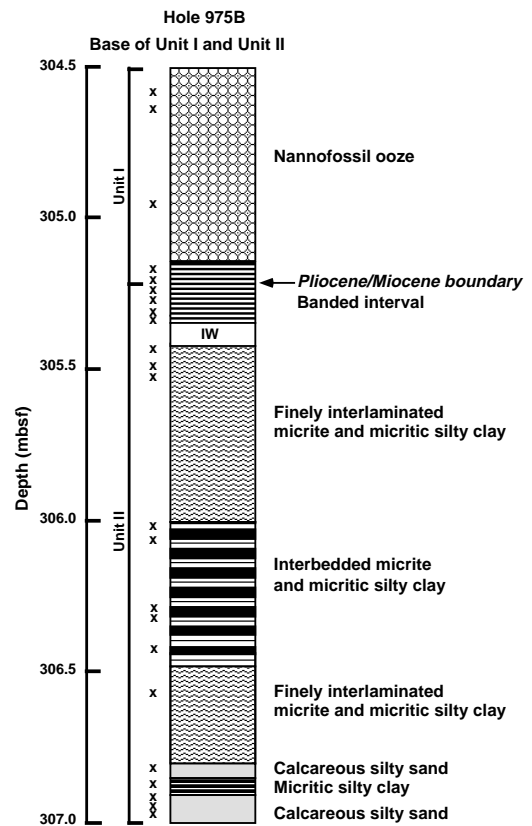


Figure 8. Generalized stratigraphic column for the base of Unit I and all of Unit II at Hole 975B. Small x's beside the column indicate the depths of XRD samples. Interval marked IW indicates the position of a whole-round interstitial water sample.

ported by water or by eolian processes (Schreiber, 1988). The finer “pure” gypsum laminae at Site 975 could represent direct precipitates at the air-water interface, or the fine gypsum could also be reworked from the basin margins and deposited in deeper water by density currents (Schreiber, 1988). The laminations are episodic, likely reflecting periods of evaporitic drawdown, and meteoric or marine influx; in modern brine ponds, as many as eight laminae may form per year (Schreiber, 1978).

Gypsum laminae exhibiting inverse grading have been ascribed in the literature to a variety of mechanisms including alternating precipitation of fine gypsum and anhydrite where the latter is subsequently replaced by coarse-grained gypsum (Ogniben, 1955), increasing grain size during direct precipitation in the water column (Garrison et al., 1978), mechanical transport and deposition of coarser particles over a finer grained substrate during storms (Hardie and Eugster, 1971), growth of gypsum at the top of laminae as a function of diagenesis (Schreiber et al., 1976), and progressive increase in size of settling crystals as a function of increasing brine concentration (Garrison et al., 1978). Garrison et al. (1978) proposed that irregular relief on planar-wavy laminations may have originated as adhesion or ripple marks and suggested that inverse grading could have been produced by backwash on a beach. Similar features are present in gypsiferous sediments described by Vonder Haar (1976) in the modern Laguna Mormona of Baja California.

We suggest that the most likely origin of the Site 975 planar-wavy and planar-cumulus laminae, and perhaps even the pinch-and-swell structures, may be early-diagenetic overgrowth of detrital gypsum at and just below the sediment-water interface. Schreiber et al. (1976) attributed similar wavy-laminated and nodular clumps of crystals to

rapid subaqueous precipitation. The globular masses that characterize the planar-cumulus structures described in this study thus are likely a product of rapid surficial crystal overgrowth. The tendency to subvertical crystal alignment in the coarser grained tops of planar-wavy and

planar-cumulus structures also supports such a mechanism in that gypsum crystals that grow as crusts at the sediment-water interface are more likely to have their long axes aligned perpendicular to bedding (Schreiber, 1988). The degree of development of surface topography (wavy vs. cumulus vs. pinch-and-swell) and crystal size in the Site 975 examples may be a function of the time between brine concentration and crystal overgrowth, and burial by matrix sediment. Surficial erosion and dissolution may also be important processes in determining the form ultimately preserved by burial. Such crystal overgrowth would result in interlocking textures, but would also allow for the preservation of larger intercrystalline pores that are present in the pinch-and-swell horizons. The draping and onlapping relationships between laminated matrix and the gypsum "swells" in the pinch-and-swell horizons suggest that the "swells" formed minor topographic highs at the sediment-water interface. Low areas were preferentially infilled with sediment. Growth of the "swells" during matrix deposition is suggested by intertonguing of matrix and coarse gypsum near swell margins. There is no evidence (e.g., inclusions of fine anhydrite or algal filaments) to suggest that the pinch-and-swell gypsum at Site 975 had a supratidal anhydrite precursor.

The sedimentary structures observed in the Site 975 gypsum section appear to represent a continuum of processes associated with the two gypsum cycles outlined in Figure 2. In these cycles there is a gradual progression in the laminate gypsum from planar to planar-wavy to planar-cumulus structures and eventually to pinch-and-swell gypsum. The pinch-and-swell gypsum is abruptly overlain by clay and gypsiferous chalk. This sequence might imply a period of time after clay deposition, when carbonate was preferentially precipitated in the overlying water mass. Much of the character of the gypsiferous chalk appears to be a function of diagenetic displacive growth of gypsum crystals within an unconsolidated sediment. The presence of laminae of densely packed subhorizontal gypsum crystals arranged in a criss-crossing palisade pattern suggests that the chalk was not deposited as a single "event" bed, but was laid down gradually with hiatuses marked by growth of gypsum-crystal crusts on the sediment surface. It is difficult to say whether the clay and gypsiferous chalk represent the beginning or the end of the process that produced the gypsum cycles. The appearance of crenulated gypsum and possible rip-clast conglomerates at the base of the recovered section at Site 975 suggest a down-section change in facies.

### Depositional Environment

Most previous workers have favored a shallow-water to supratidal (sabkha) depositional environment for the Messinian sedimentary

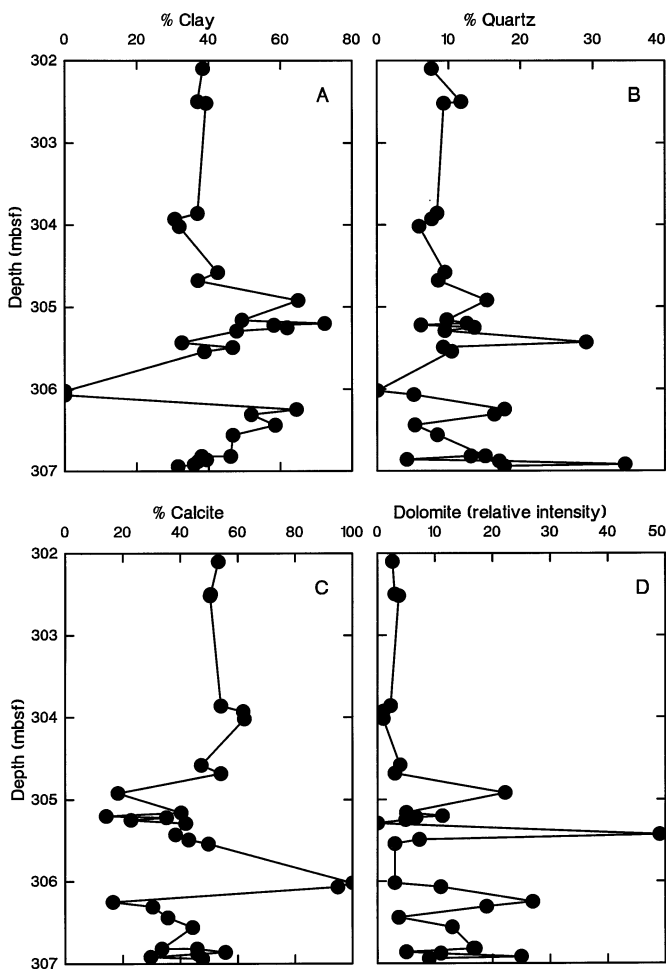


Figure 9. Depth profiles of abundances of some of the major phases quantified by XRD for sediments from Unit II and the base of Unit I from Hole 975B. A. Clay minerals. B. Quartz. C. Calcite. D. Dolomite.

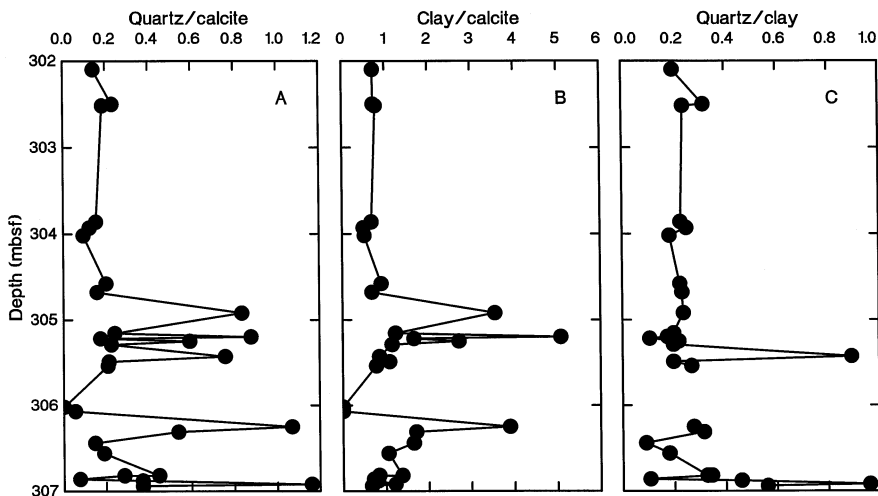


Figure 10. Depth profiles of mineral ratios for sediments from Unit II and the base of Unit I from Hole 975B. A. Quartz/calcite. B. Clay/calcite. C. Quartz/clay. The gap in the data around 306 mbsf in (C) corresponds to samples with no X-ray detectable clay minerals.

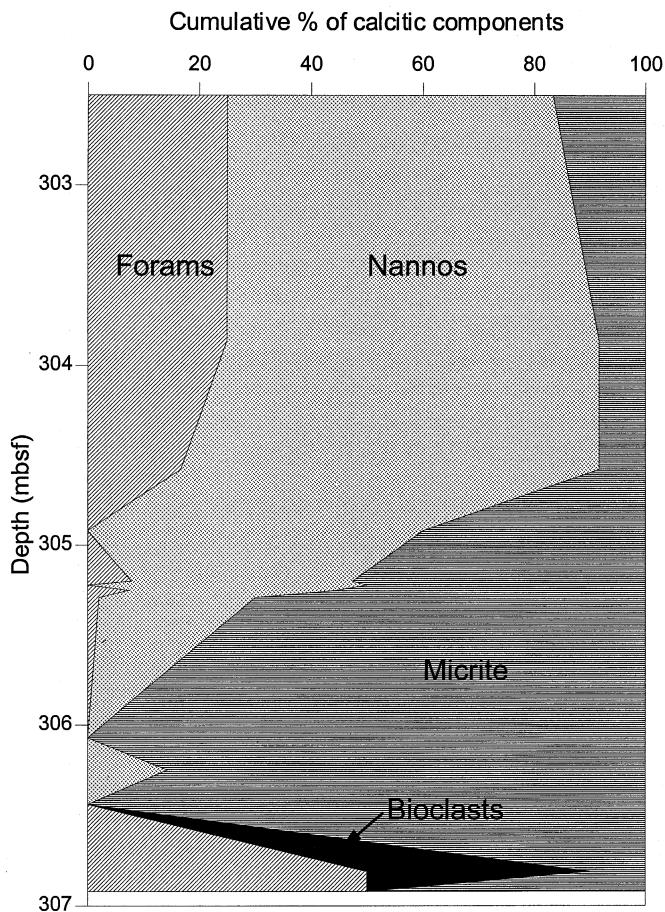


Figure 11. Depth variations in the relative abundances of calcitic components identified in smear slides for Unit II and the base of Unit I from Hole 975B, expressed in terms of cumulative area percent (data from Comas, Zahn, Klaus, et al., 1996).

section (e.g., Garrison et al., 1978). There are, however, conflicting opinions as to whether the basin was shallow or deep (see Sonnenfeld, 1985). Evidence cited by Nesteroff (1973) in favor of a deep depositional basin include the deep-water fauna in the earliest Pliocene sedimentary fill and the presence of deeply cut submarine canyon systems and terrigenous coarse clastic sand within the basins. Criteria called upon by Nesteroff (1973), Nesteroff et al. (1973), and Friedman (1973) to support shallow-water to supratidal (sabkha) deposition include: laminated stromatolitic structures, nodular to chicken-wire anhydrite, littoral or brackish benthic microfaunas (foraminifers, ostracodes, diatoms), isotopic studies (e.g., Fontes et al., 1973) and the presence of halite and dolomite.

In our shipboard analysis of the Site 975 sequence, we tentatively compared the gypsum cycles at Site 975 to evaporite cycles defined by Garrison et al. (1978) for Site 374 in the Ionian Sea (Fig. 1) and suggested that they formed in a supratidal to shallow, subaqueous environment. Closer inspection shows significant differences between the Site 374 and Site 975 facies. For example, in the cycles at Site 374, the basal member consists of dolomitic to diatomaceous mudstone, in some cases displaying stromatolitic-like laminations. Displacive crystals and pinch-and-swell structures of gypsum, interpreted to have replaced anhydrite, disrupt the fabric of the mudstones. In contrast, the clays and micritic silty clays interbedded with the gypsum at Site 975 are calcitic and do not have textures or displacive fabrics similar to those of the mudstones at Site 374. The gypsiferous chinks of Site 975 are somewhat similar in appearance to some of the more disrupted mudstones at Site 374, but again, the chinks at Site 975 are calcitic, not dolomitic. Furthermore, the pinch-and-swell

evaporites at Site 374 consist of anhydrite or gypsum after anhydrite that formed displacively in a carbonate mud. As stated above, we see no evidence for anhydrite precursor mineralogy in the pinch-and-swell gypsum at Site 975. The pinch-and-swell gypsum at Site 975 is also relatively pure gypsum, with only low concentrations of calcite, quartz, or dolomite (Table 3).

The Messinian evaporite sequence recovered at Site 372 (Menorca Rise, Fig. 1), contains evaporite lithofacies similar to those at Site 975. Although there are differences between the two sites in the carbonate facies and in the cyclic sequence of evaporite lithofacies, the clastic and crystalline textures in the laminated to "micro-laminated" gypsum intervals in Core 8 at Site 372 are nearly identical to those found in the planar, planar-wavy, and planar-cumulus laminated intervals at Site 975. The evaporite sequence at Site 372 contains cross-laminated intervals and better developed crenulated and intraclastic (rip-up) beds; noticeably lacking, however, is the more massive, pinch-and-swell gypsum present at Site 975. This lithofacies may be present at Site 372, but not recovered. Garrison et al. (1978) interpreted the Site 372 evaporites as having been deposited on a shallow-water evaporite flat or lagoon above storm wave base and within the photic zone.

We believe that our textural and sedimentological evidence, coupled with the sequential change from planar to planar-wavy to planar-cumulus to pinch-and-swell gypsum in the cycles at Site 975, suggests a subaqueous origin for the evaporative facies. Current data provide no evidence for a supratidal or sabkha-type environment. Laminated evaporites can be the product of intertidal, shallow-water, or deep water-processes. Lateral continuity of gypsum laminae is often used as an indication of deep-water basinal deposition (see Warren, 1983, for discussion). Our view at Site 975 is limited to a few centimeters within the core. However, we are fortunate that the ship's position was offset 20 m to the north after drilling Hole 975B and before drilling Hole 975C, and a unique sequence of evaporite beds can be directly correlated between the two holes. As Figure 4A, B indicates, there is a direct correlation of pinch-and-swell gypsum, clay and gypsiferous chalk across this interval and the finest details in overlying and underlying gypsum laminae are also directly correlative on a millimeter-scale.

Additionally, we observed no cross stratification, desiccation features, brine shrimp fecal pellets, algal filaments, or cerithid gastropods that would indicate, as suggested by Schreiber et al. (1976) and Schreiber (1988), a shallow-water origin. Thus, our observations are consistent with a deeper water depositional setting for the accumulation of these sediments, where "deep" is defined only as below wave base. The question of whether or not these sediments accumulated within the photic zone as discussed in Schreiber et al. (1976), could only be answered by using a scanning electron microscope to establish the presence or absence of fine algal structures. In fact, within a laminated interval (Section 161-975B-33X-CC, 22–27 cm), we observed circular pores in fine gypsum crystals that could either be dissolved nanofossils or possibly coccooid algae (see Awramik, 1978).

The submillimeter to fine millimeter-scale laminations observed in the laminated gypsum at Site 975 could represent various basin-wide, climatic phenomena such as seasonal changes in temperature, precipitation, and humidity, or perhaps even singular rainfall events or pulses of seawater input into the basin that decrease salinity and result in carbonate precipitation (Warren, 1983).

Across the Mediterranean, the marly interbeds of the upper Miocene are characterized by dwarfed marine foraminiferal and oligotypical faunas that probably are the result of ecologic stress (Cita, 1973; Hsü, Montadert, et al., 1978). In addition to foraminifers within gypsiferous chalk beds at Site 975, we have found whole and/or fragmented foraminifers in almost every matrix (gypsum) lamina examined in this study. This seems to imply that the marine incursions thought to be responsible for the interbedded marls may have in fact been stronger signals of continuous seawater influx into the basin during the latest Messinian. The alternative explanation, that these foraminifers could be eolian contamination from exposed marine

facies on the margin of the basin, is probably best evaluated by detailed paleontological studies.

### Post-Evaporite Sandstone Provenance and Depositional Setting

The calcareous and mixed calcareous/terrigenous sand interval (Core 161-975B-33X-CC, 3–11 cm) recovered from Hole 975B may grade laterally into a pebbly sand. At Hole 975C (offset of 20 m), a pebble 4.5 cm in diameter, but no sand, was recovered in this interval. In thin section, the pebble consists of tectonized granule conglomerate, with twinned carbonate cement and clasts of quartz, quartzite, metaquartzite, and chert. The composition of terrigenous material in this sandy unit, particularly the common presence of siliciclastic and metamorphic lithic grains, is consistent with derivation from Paleozoic sedimentary, metasedimentary, and schistose basement rocks that crop out on Menorca and have been dredged from off Menorca (Bourrouilh and Gorsline, 1979; Jenkyns et al., 1990).

In contrast, the carbonate- and volcanic-lithic suite found in the sand at Section 161-975B-33X-3, 141–144 cm, could easily be attributed to the erosional products of Mesozoic rocks exposed on the island of Menorca. The Triassic section on Menorca includes red-bed siliciclastic rocks, dolomites, intertidal and subtidal carbonates, evaporites and alkaline mafic volcanic and pyroclastic rocks (Jenkyns et al., 1990; Rodríguez-Perea et al., 1987). This sequence is in turn overlain by Jurassic platform carbonates that include stromatolitic, pelletal, and intraclastic facies, followed by pelagic carbonates that locally include red nodular limestone (*ammonitico rosso*), and Fe-Mn hardgrounds (Jenkyns et al., 1990; Rodríguez-Perea et al., 1987). At Site 122 to the north of the Balearic Islands in the Valencia Trough, gravel recovered just above Messinian evaporites (Ryan, Hsü et al., 1973) is amazingly similar in composition to the volcaniclastic sandy interval described at Site 975 (Section 975B-33X-3, 141–144 cm). Thus, it is possible that Site 975 and Site 122 both received detritus from an uplifted Mesozoic section on Menorca during the latest Miocene.

Messinian evaporite sequences throughout the region are commonly overlain by foraminifer- and quartz-bearing sandy intervals (Fig. 1; e.g., Sites 371 and 372 [Hsü, Montadert, et al., 1978]; Sites 124 and 132 [Ryan, Hsü, et al., 1973]; Sicily [Hsü et al., 1973]). At Site 975, the basal post-evaporite sand facies is likely a product of increased input of marine water into the South Balearic region, as suggested by the abundance of foraminifers. The sandstone bed is laminated and moderately well sorted, and could be the result of a catastrophic flooding event (e.g., like that envisioned by Cita et al., 1978) or alternatively of eolian or beach processes acting along the margin of a rising proto-Balearic Sea. The abrupt up-section shift from sand composed of foraminifers and terrigenous debris to sand composed of carbonate- and volcanic-lithic debris remains problematic.

### Origin of Post-Evaporite Micritic Carbonate

The sediments of Unit II at Site 975 have a number of distinctive characteristics that distinguish them from Messinian post-evaporite deposits at other drilling sites:

1. Carbonate mineralogy. Unit II sediments are calcitic; dolomite is present in only minor amounts throughout the unit (Table 2). In contrast, dolomitic marls characterize many of the Messinian carbonate sediments recovered during previous drilling legs in the region (e.g. Sites 124, 132, and 134 [Ryan, Hsü, et al., 1973]; Site 374 [Garrison et al., 1978]);
2. Nature of the calcite. The Site 975 micrites consist of silt-sized, lens-shaped grains of calcite that appear to be inorganic in origin. The Messinian calcitic marl oozes from other drilling sites contain predominantly biogenic calcite, although some micrite has been noted (e.g., Site 132, Ryan, Hsü, et al., 1973);

3. Abundance of microfossils. Nannofossils and foraminifers are rare to absent in the micrites at Site 975. Diatoms, found at a few other drilling sites, are absent in the Unit II sediments of Site 975; and
4. Terrigenous content. Terrigenous input to the Unit II depositional environment was highly variable temporally. The pure micrites of Site 975 Unit II contain only traces of terrigenous material. None of the other drilling legs in the region recovered sediment of Messinian age comparable to the pure micrite of Unit II.

The micritic sediments of Unit II appear to have formed in an environment characterized by inorganic calcite precipitation, low planktonic productivity, and episodic, variable influx of terrigenous material. Only during times of isolation from the terrigenous sediment sources could pure micrite accumulate. The lack of bioturbation throughout Unit II indicates an absence of benthic burrowing fauna. Ostracodes and the benthic foraminifer *Ammonia tepida* found in Section 161-975B-33X-CC (Shipboard Scientific Party, 1996b) indicate a brackish-water environment for the sediments at the base of Unit II. In addition, foraminifers from Sample 975B-33X-3, 80 cm, to the bottom of the hole are dwarfed forms, indicative of a stressed environment.

In the Site 975 chapter (Shipboard Scientific Party, 1996b), it was suggested that the micritic sediments were deposited in a shallow-water, low-energy, environment, and that the fine laminations that characterize all but the most clay-rich intervals could be due to either (1) seasonal fluctuations of productivity, salinity, or terrigenous input, or (2) layering of algal/microbial mats. An alternative interpretation of origin is suggested by the similarity of the pure micrites to chemically precipitated lacustrine chalks such as those described by Hsü and Kelts (1978) from the Black Sea. These chalks are thought to have formed in a deep, largely stagnant, freshwater lake. Additional paleontological analyses, as well as scanning electron microscopic investigations and isotopic analyses (both currently in progress) are necessary to refine further an interpretation of the depositional environment of the Unit II micritic sediment.

## CONCLUSIONS

On the basis of detailed petrographic observations, we propose that the gypsum-bearing sediments of Unit III at Site 975 were deposited in a subaqueous environment, below wavebase. The planar-laminated gypsum appears to be detrital in origin, and the laminations reflect episodic fluctuations in the balance of evaporation and influx of meteoric or marine waters. The wavy-planar and planar-cumulus laminated facies, and perhaps also the pinch-and-swell gypsum facies, are thought to have formed by early-diagenetic overgrowth of the detrital planar gypsum at, or just below, the sediment-water interface. The deposition and diagenetic overprinting of the gypsum facies was periodically punctuated by influx of matrix sediment. The gypsiferous chalk facies is thought to have formed by displacive, diagenetic growth of gypsum crystals from the gypsum-saturated pore waters of a carbonate sediment.

These gypsum facies, along with intervals of clay and micritic silty clay, are present at Site 975 in cycles.

A possible scenario of formation of these cycles, in the context of a deep (below wavebase) basin with periodic marine influx, is as follows (moving upsection):

1. Basal clay: high influx of marine water; deepest and least saline conditions; minor carbonate or gypsum precipitation;
2. Gypsiferous chalk: increasing evaporation; carbonate precipitation dominated with in situ diagenetic growth of gypsum; and
3. Laminated to pinch-and-swell gypsum: increasing salinity; deposition of detrital gypsum (precipitated at air-water inter-

face?) followed by extensive diagenetic overgrowth. Isotopic and chemical analyses, currently in progress, will help clarify the changes in environmental conditions during formation of these gypsum cycles,

The gypsum-dominated sediments of Unit III are capped by the laminated calcareous/terrigenous sand at the base of Unit II, a thin interval of micrite-rich sediment, and a layer of graded, calcareous-volcaniclastic sand. These sand layers reflect influx of exotic sediment and mark significant depositional events in the history of this section. Deposition of the sands was accompanied by influx of water to the basin, either marine waters from the west, or perhaps meteoric waters from lacustrine environments to the east.

The influx of the waters from which the sands were deposited resulted in cessation of gypsum deposition, and a shift to calcite precipitation. The interlaminated and interbedded micrites and micritic silty clays of Unit II reflect periodic, variable magnitude, influx of terrigenous sediment to a calcite precipitating basin. The light and dark bands that characterize the Miocene/Pliocene boundary interval are perhaps just subtle versions of the micritic and clay-dominated layers downsection and may reflect the final sedimentological fluctuations before fully marine conditions of the Pliocene were established. Detailed paleontological work on samples from the sandy intervals of Unit II and isotopic analyses on overlying micritic sediments should shed light on their origins and the implications for changes in depositional environments during the terminal stages of the Messinian and the transition to the open-marine environment of the lower Pliocene at Site 975.

#### REFERENCES

- Awramik, S.M., 1978. Stromatolites with coccoid and filamentous blue-green algae of Messinian age from Site 374, Ionian Abyssal Plain. *In* Hsü, K.J., Montadert, L., et al., *Init. Repts. DSDP*, 42 (Pt. 1): Washington (U.S. Govt. Printing Office), 665–668.
- Bourrouilh, R., and Gorsline, D.S., 1979. Pre-Triassic fit and Alpine tectonics of continental blocks in the western Mediterranean: *Bull. Geol. Soc. Am.*, 90:1074–1083.
- Carozzi, A.V., 1993. *Sedimentary Petrography*: Englewood Cliffs, NJ (Prentice Hall).
- Cita, M.B., 1973. Inventory of biostratigraphical finding and problems. *In* Ryan, W.B.F., Hsü, K.J., et al., 1973. *Init. Repts. DSDP*, 13: Washington (U.S. Govt. Printing Office), 1045–1074.
- Cita, M.B., Ryan, W.B., and Longinelli, A., 1978. Messinian paleoenvironments. *In* Hsü, K.J., Montadert, L., et al., *Init. Repts. DSDP*, 42 (Pt. 1): Washington (U.S. Govt. Printing Office), 1003–1035.
- Comas, M.C., Zahn, R., Klaus, A., et al., 1996. *Proc. ODP, Init. Repts.*, 161: College Station, TX (Ocean Drilling Program).
- Fontes, J.C., Letolle, R., Nesteroff, W.D., and Ryan, W.B., 1973. Oxygen, carbon, sulfur, and hydrogen stable isotopes in carbonate and sulfate mineral phases of Neogene evaporites, sediments and in interstitial waters, Leg 13. *In* Ryan, W.B.F., Hsü, K.J., et al., *Init. Repts. DSDP*, 13: Washington (U.S. Govt. Printing Office), 788–796.
- Friedman, G.M., 1973. Petrographic data and comments on the depositional environment of the Miocene sulfates and dolomites at Sites 124, 132 and 134, western Mediterranean Sea. *In* Ryan, W.B.F., Hsü, K.J., et al., *Init. Repts. DSDP*, 13: Washington (U.S. Govt. Printing Office), 695–708.
- Garrison, R.E., Schreiber, B.C., Bernoulli, D., Fabricius, F.H., Kidd, R.B., and Mélières, F., 1978. Sedimentary petrology and structures of Messinian evaporitic sediments in the Mediterranean Sea, Leg 42A, Deep Sea Drilling Project. *In* Hsü, K.J., Montadert, L., et al., *Init. Repts. DSDP*, 42 (Pt. 1): Washington (U.S. Govt. Printing Office), 571–611.
- Hardie, L.A., and Eugster, H.P., 1971. The depositional environment of marine evaporites: a case for shallow water clastic accumulation. *Sedimentology*, 16:187–220.
- Hsü, K.J., Cita, M.B., and Ryan, W.B.F., 1973. The origin of the Mediterranean evaporites. *In* Ryan, W.B.F., Hsü, K.J., et al., *Init. Repts. DSDP*, 13 (Pt. 2): Washington (U.S. Govt. Printing Office), 1203–1231.
- Hsü, K.J., and Kelts, K., 1978. Late Neogene sedimentation in the Black Sea. *In* Matter, A., and Tucker, M.E., *Modern and Ancient Lake Sediments*: Oxford (Blackwell Scientific), *IAS Spec. Publ.*, 129–145.
- Hsü, K.J., Montadert, L., et al., 1978. *Init. Repts. DSDP*, 42 (Pt. 1): Washington (U.S. Govt. Printing Office).
- Jenkyns, H.C., Sellwood, B.W., and Pomar, L., 1990. A field excursion guide to the Island of Mallorca. *Geol. Assoc. Guide*, 42.
- Karлак, R.F., and Burnett, D.S., 1966. Quantitative phase analysis by X-ray diffraction. *Anal. Chem.*, 38:1741–1745.
- Nesteroff, W.D., 1973. Mineralogy, petrography, distribution, and origin of the Messinian Mediterranean evaporites. *In* Ryan, W.B.F., Hsü, K.J., et al., *Init. Repts. DSDP*, 13: Washington (U.S. Govt. Printing Office), 673–694.
- Nesteroff, W.D., Wezel, F.C., and Pautot, G., 1973. Summary of lithostratigraphic findings and problems of evaporites. *In* Ryan, W.B.F., Hsü, K.J., et al., *Init. Repts. DSDP*, 13: Washington (U.S. Govt. Printing Office), 1021–1040.
- Ogniben, L., 1955. Inverse graded bedding in primary gypsum of chemical deposition. *J. Sediment. Petrol.*, 25:273–281.
- Pierre, C., and Fontes, J.C., 1978. Isotope composition of Messinian sediments from the Mediterranean sea as indicators of paleoenvironments and diagenesis. *In* Hsü, K.J., Montadert, L., et al., *Init. Repts. DSDP*, 42: Washington (U.S. Govt. Printing Office), 635–650.
- Richter-Bernburg, G., 1973. Facies and paleogeography of the Messinian evaporites of Sicily. *In* Drooger, C.W., et al. (Eds.), *Messinian Events in the Mediterranean. Geodyn. Sci. Rep.*, 7:124–141.
- Rodríguez-Perea, A., Ramos-Guerrero, E., Pomar, L., Paniello, X., Obrador, A., and Martí, J., 1987. El Triasico de las Baleares. *Cuadernos Geol. Iber.*, 11:295–321.
- Ryan, W.B.F., Hsü, K.J., et al., 1973. *Init. Repts. DSDP*, 13 (Pts. 1 and 2): Washington (U.S. Govt. Printing Office).
- Schreiber, B.C., 1978. Environments of subaqueous gypsum deposition. *In* Dean, W.E., and Schreiber, B.C. (Eds.), *Marine Evaporites. SEPM Short Course*, 4:43–73.
- , 1988. *Evaporites and Hydrocarbons*: New York (Columbia Univ. Press).
- Schreiber, B.C., Friedman, G.M., Decima, A., and Schreiber, E., 1976. Depositional environments of Upper Miocene (Messinian) evaporite deposits of the Sicilian basin. *Sedimentology*, 23:729–760.
- Shipboard Scientific Party, 1996a. Explanatory notes. *In* Comas, M.C., Zahn, R., Klaus, A., et al., *Proc. ODP, Init. Repts.*, 161: College Station, TX (Ocean Drilling Program), 21–49.
- Shipboard Scientific Party, 1996b. Site 975. *In* Comas, M.C., Zahn, R., Klaus, A., et al., *Proc. ODP, Init. Repts.*, 161: College Station, TX (Ocean Drilling Program), 113–177.
- Sonnenfeld, P., 1985. Models of late Miocene evaporite genesis in the Mediterranean region. *In* Stanley, D.J., and Wezel, F.-C. (Eds.), *Geological Evolution of the Mediterranean Basin*: New York (Springer-Verlag), 323–346.
- Vonder Haar, S.P., 1976. Evaporites and algal mats at Laguna Mormona, Pacific Coast, Baja California, Mexico [Ph.D. thesis]. Univ. of Southern California.
- Warren, J.K., 1983. On the significance of evaporite lamination. *Sixth Int. Symp. on Salt*, 1:161–169.
- Wilkens, R.H., DeCarlo, E.H., and Tribble, J.S., 1992. Data report: X-ray bulk mineralogy of Exmouth and Wombat Plateau sediments, northwest Australian margin. *In* von Rad, U., Haq, B.U., et al., *Proc. ODP, Sci. Results*, 122: College Station, TX (Ocean Drilling Program), 887–896.

**Date of initial receipt: 8 May 1997**

**Date of acceptance: 2 December 1997**

**Ms 161SR-201**

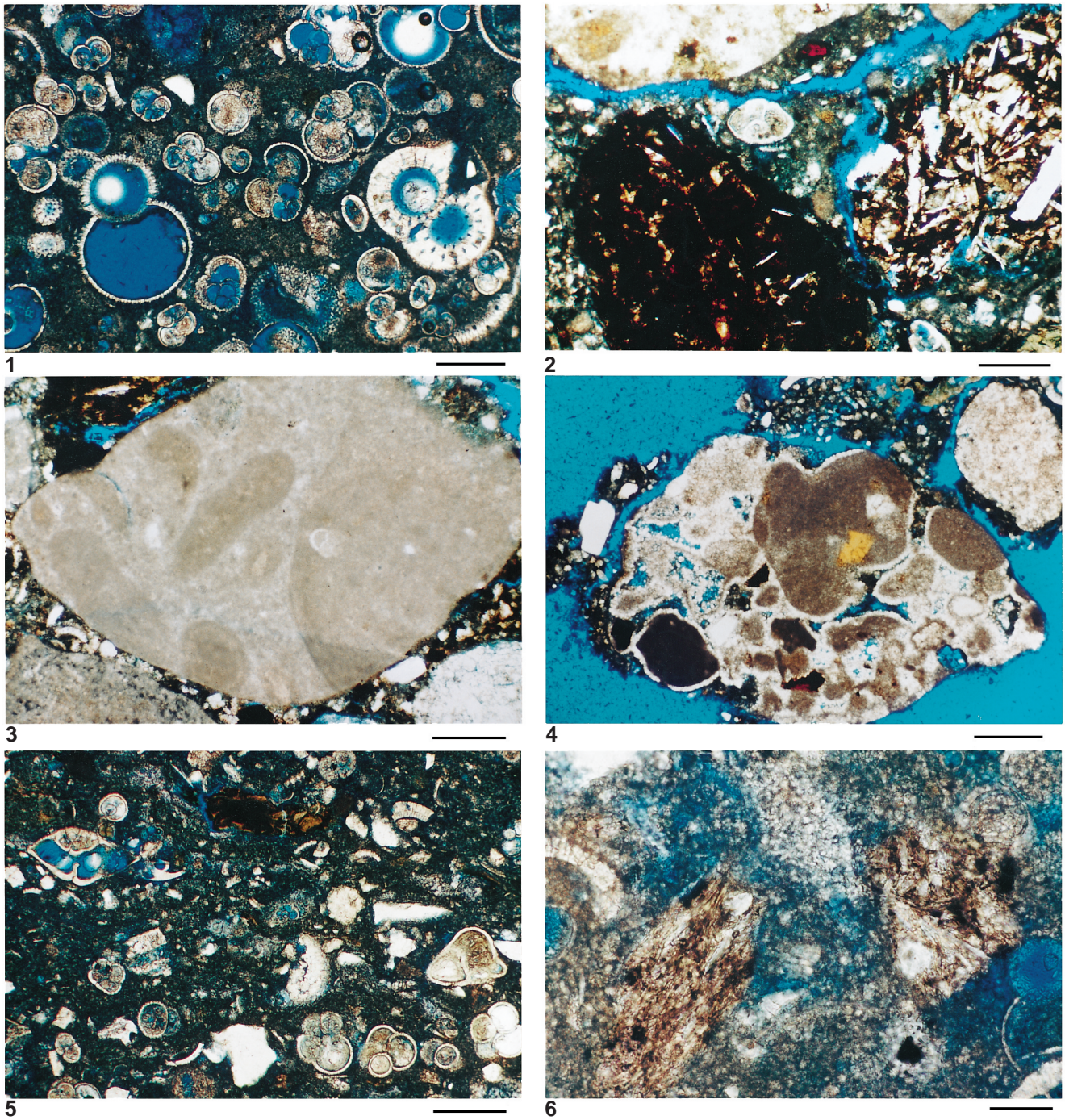
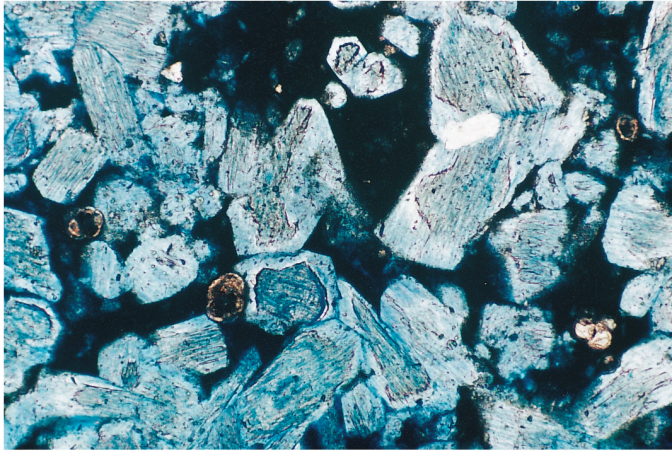
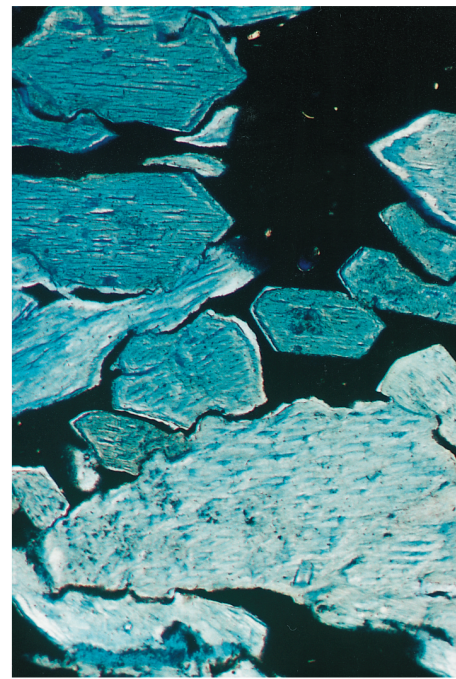


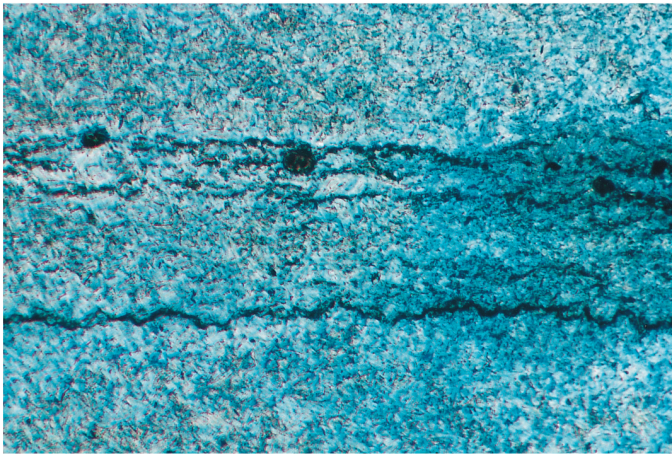
Plate 1. Photomicrographs. **1.** General view of foraminiferal-nannofossil chalk. Section 161-975B-33X-2, 3–4 cm. Scale bar is 0.1 mm. **2.** Black (tachylitic) microlitic and lathwork volcanic lithic fragments. Section 975B-33X-3, 143–144 cm. Scale bar is 0.1 mm. **3.** Carbonate lithic fragment exhibiting pelletal to oncolitic(?) texture. Section 975B-33X-3, 143–144 cm. Scale bar is 0.1mm. **4.** Carbonate lithic fragment of calcarenite with drusy rim cement. Section 975B-33X-3, 143–144 cm. Scale bar is 0.2 mm. **5.** General view of matrix-supported sandy biomicrite. Section 975B-33X-CC, 3–5 cm. Scale bar is 0.1 mm. **6.** Two fragments of shale/siltstone in matrix-rich area. Section 975B-33X-CC, 3–5 cm. Scale bar is 0.05 mm.



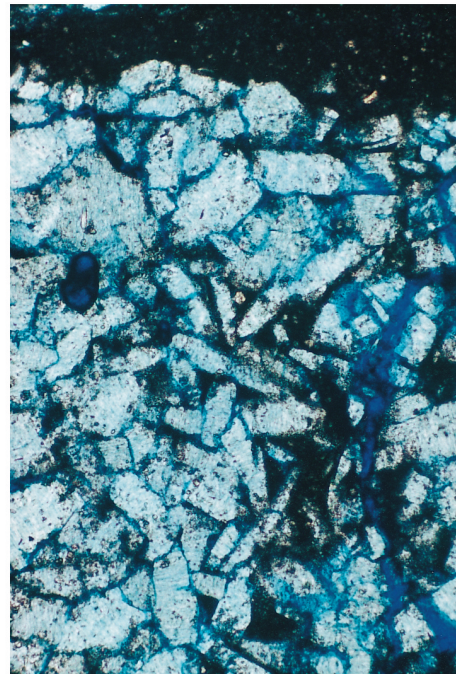
1



2



3



4

Plate 2. Photomicrographs. **1.** Gypsiferous chalk with sparse, whole foraminifers, Section 161-975B-34X-2, 7–11 cm. Apparent zoning is likely an artifact of sample preparation where the gypsum is altering to bassanite ( $\text{CaSO}_4 \cdot \frac{1}{2}\text{H}_2\text{O}$ ; S. Hovorka, pers. comm., 1996). Scale bar is 0.1 mm. **2.** Gypsiferous chalk with large euhedral to anhedral gypsum crystals that have undergone pressure solution where in contact with each other, producing stylolitic contacts. Section 975B-34X-2, 21–25 cm. Scale bar is 0.2 mm. **3.** Finely laminated gypsum with thin submillimeter laminae of matrix that appear as dark, stylolitic seams. Dark spots along matrix seam are foraminifers. Scale bar is 0.1 mm. **4.** Clastic interval containing fragments of lenticular gypsum within crenulated gypsum zone pictured in Figure 6. Section 975B-34X-CC, 15–19 cm. Scale bar is 0.2 mm.

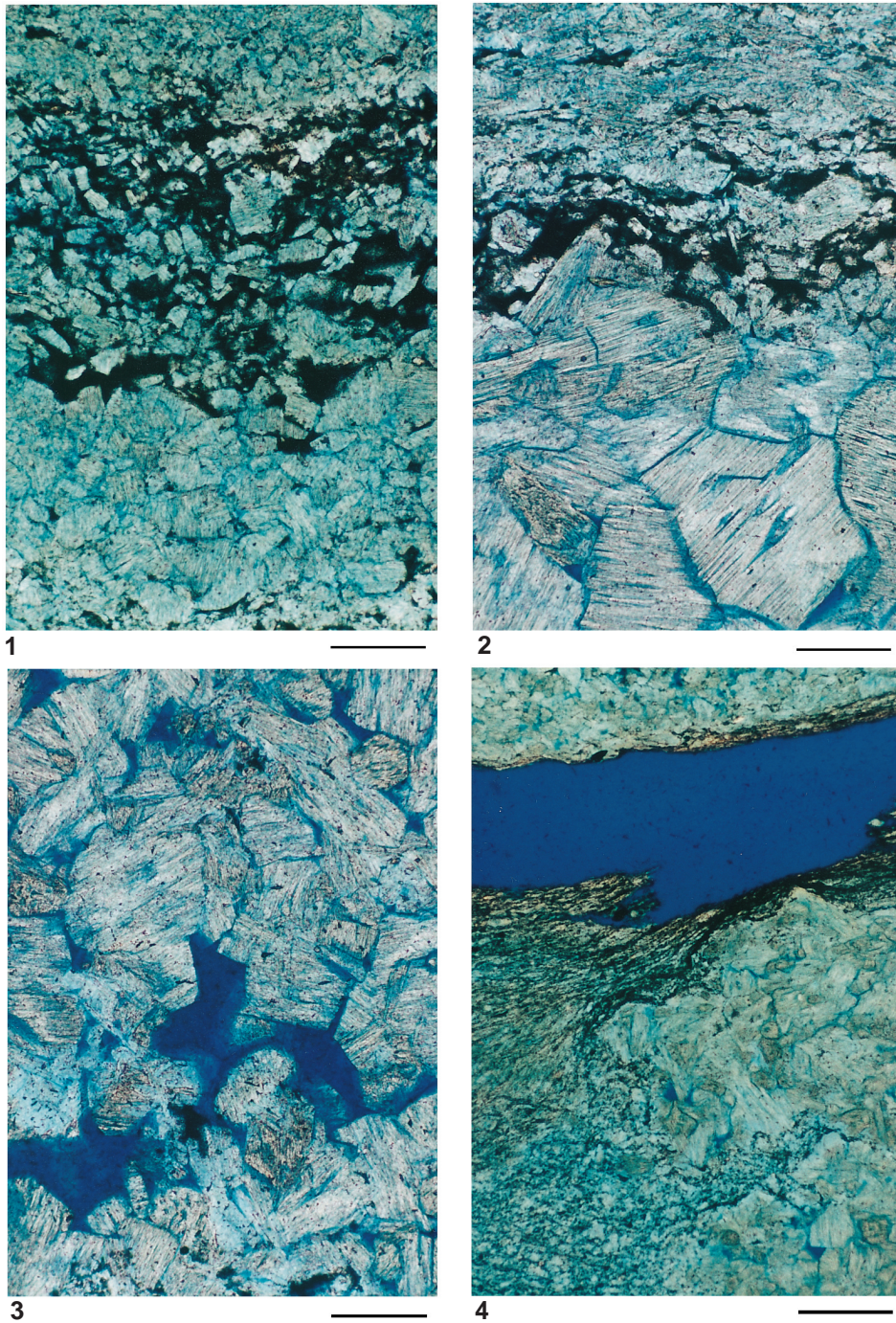


Plate 3. Photomicrographs. **1.** Planar-wavy lamina with clastic texture (lower part of picture) is overlain by dark, matrix-rich lamina with detrital gypsum. Lenticular crystals are present in both laminae. Section 161-975B-33X-CC, 15–19 cm. Scale bar is 0.1 mm. **2.** Coarse, interlocking crystals of gypsum in lower half of picture are the uppermost part of a planar-cumulus lamina overlain by a dark, matrix lamina with detrital gypsum. Section 975B-33X-CC, 22–27 cm. Scale bar is 0.1 mm. **3.** Large intercrystalline pores in coarsely crystalline gypsum pinch-and-swell structure. Section 975B-34X-1, 26–30 cm. Scale bar is 0.1 mm. **4.** Sample split along matrix-rich seam producing large epoxy-filled fracture seen in upper part of photograph. Fine lamination and detrital grains within the matrix-rich drape (left) interfinger and cover coarse, interlocking gypsum crystals in pinch-and-swell structure (right). For clarification, see core photograph in Figure 7. Section 975B-34X-1, 26–30 cm. Scale bar is 0.2 mm.